



Interpretation of the near-IR spectra of the Kuiper Belt Object (136472) 2005 FY₉

Janusz Eluszkiewicz,¹ Karen Cady-Pereira,¹ Michael E. Brown,² and John A. Stansberry³

Received 9 January 2007; revised 26 February 2007; accepted 5 April 2007; published 15 June 2007.

[1] Visible and near-IR observations of the Kuiper Belt Object (136472) 2005 FY₉ have indicated the presence of unusually long (1 cm or more) optical path lengths in a layer of methane ice. Using microphysical and radiative transfer modeling, we show that even at the frigid temperatures in the outer reaches of the solar system, a slab of low-porosity methane ice can indeed form by pressureless sintering of micron-sized grains, and it can qualitatively reproduce the salient features of the measured spectra. A good semiquantitative match with the near-IR spectra can be obtained with a realistic slab model, provided the spectra are scaled to a visible albedo of 0.6, at the low end of the values currently estimated from *Spitzer* thermal measurements. Consistent with previous modeling studies, matching spectra scaled to higher albedos requires the incorporation of strong backscattering effects. The albedo may become better constrained through an iterative application of the slab model to the analysis of the thermal measurements from *Spitzer* and the visible/near-IR reflectance spectra. The slab interpretation offers two falsifiable predictions: (1) Absence of an opposition surge, which is commonly attributed to the fluffiness of the optical surface. This prediction is best testable with a spacecraft, as Earth-based observations at true opposition will not be possible until early next century. (2) Unlikelihood of the simultaneous occurrence of very long spectroscopic path lengths in both methane and nitrogen ice on the surface of any Kuiper Belt Object, as the more volatile nitrogen would hinder densification in methane ice.

Citation: Eluszkiewicz, J., K. Cady-Pereira, M. E. Brown, and J. A. Stansberry (2007), Interpretation of the near-IR spectra of the Kuiper Belt Object (136472) 2005 FY₉, *J. Geophys. Res.*, 112, E06003, doi:10.1029/2007JE002892.

1. Introduction

[2] From the recently reported visible and near-IR observations of the Kuiper Belt Object (136472) 2005 FY₉, *Licandro et al.* [2006] and *Brown et al.* [2007] have inferred that methane ice is the dominant component of the surface (for brevity, in the remainder of this paper we will refer to this object as “2005 FY₉”). Moreover, both groups concluded that methane is very coarse-grained, with the grain size (interpreted as the mean distance between scattering centers in the ice) on the order of 1 cm according to a Hapke-type modeling carried out by *Brown et al.* [2007]. Even larger grains (up to several centimeters) were employed by *Tegler et al.* [2007] to match their visible spectra. Such large grain sizes are indicative that methane ice is present as a low-porosity slab rather than a fluffy frost over large portions of the surface. This discovery has put 2005 FY₉ into the same class as Triton, Pluto, and Mars, where the main volatile component (nitrogen or CO₂) also

forms dense slabs on the surface [*Cruikshank et al.*, 1984; *Owen et al.*, 1993; *Kieffer et al.*, 2000]. 2005 FY₉ also bears some similarity to Sedna, where unusually long path lengths (>10 cm) in nitrogen ice have been inferred [*Barucci et al.*, 2005; *Emery et al.*, 2007]. What makes the case of 2005 FY₉ somewhat surprising in this regard is that methane ice is not very volatile at the low temperatures in the outer reaches of the solar system. However, as shown in this paper, even at those frigid temperatures low-porosity methane-ice slabs can indeed form by pressureless sintering on timescales comparable to the orbital period, provided the methane grains are sufficiently small (in the micron range). Furthermore, we apply a recently developed model of the reflectivity of porous icy slabs to demonstrate that such a model can naturally reproduce the broad absorption features of methane ice (particularly in the 1.7-micron region) that distinguish the near-IR spectra of 2005 FY₉ from the spectra of Pluto and Eris, where methane ice is only moderately coarse-grained (grain size $\sim 100\text{--}200\ \mu\text{m}$) [*Brown et al.*, 2007; *Olkin et al.*, 2007]. It should be noted that our primary goal in this paper is to reproduce an end-member spectrum that reproduces the salient features of the observed near-IR spectra under realistic assumptions concerning the microphysical texture of 2005 FY₉'s surface. Given our microphysical focus, we do not extend our modeling beyond $2.2\ \mu\text{m}$, where additional trace absorbers have been identified by *Brown et al.* [2007], or into the visible, where a separate “red” continuum would

¹Atmospheric and Environmental Research, Inc., Lexington, Massachusetts, USA.

²Division of Geological and Planetary Sciences, California Institute of Technology, Pasadena, California, USA.

³Steward Observatory, University of Arizona, Tucson, Arizona, USA.

have to be considered. As more measurements of 2005 FY₉ become available (in particular, tighter constraints on the absolute albedo and an extended range of solar phase curve), more detailed modeling will be warranted.

2. Densification of Porous Methane Ice

[3] The basic premise of this work is that a low-porosity layer of solid methane ice is indeed present on 2005 FY₉'s surface. Barring formation by melting and refreezing (which would require temperatures in excess of 90 K in the shallow subsurface), the formation of such a layer is expected on thermodynamical grounds, given that zero porosity is the state of minimum surface energy. The kinetics of sintering and densification as it applies to solar system ices has been discussed extensively in a series of publications [Eluszkiewicz, 1991, 1993; Eluszkiewicz *et al.*, 1998, 2005; Eluszkiewicz and Moncet, 2003] and only a basic description will be given here, with the purpose of establishing broad constraints on the grain and void size for our spectral modeling. In the absence of external pressure (e.g., on the optical surface of a planet), densification is driven by surface tension, with the main driving mechanisms being volume and grain boundary diffusion. The rates of densification by these mechanisms have been worked out by Swinkels and Ashby [1981, Table 2], to whom the reader is referred for a detailed discussion of the underlying assumptions. In a modified form, given in an internal report by Ashby [1988], the rate of densification in a medium composed of spherical grains with radius r can be expressed as

$$-\frac{d\varphi}{dt} = 72C(1 - \varphi_0) \frac{D_v}{r^2} \frac{\gamma\Omega}{rkT} + 18C \frac{1 - \varphi}{\varphi_0 - \varphi} \frac{\delta_b D_b}{r^3} \frac{\gamma\Omega}{rkT} \quad (1)$$

where φ is the porosity, φ_0 is the uncompressed porosity (it is assumed that, as a result of grain rearrangement and/or adhesion, φ is smaller than φ_0 from the start of sintering), $C \equiv \varphi_0/(\varphi_0 - \varphi)$, $D_v \equiv D_{ov} \exp(-E_v/R/T)$ and $D_b \equiv D_{ob} \exp(-E_b/R/T)$ are the volume (lattice) and grain boundary diffusivities, respectively, R is the gas constant, T is the temperature, δ_b is the grain boundary width, γ is the solid-state surface tension, Ω is the molecular volume, and k is the Boltzmann constant. The material parameters for solid methane are taken from Eluszkiewicz [1991, Table 1]. Equation (1) applies to the so-called initial stage of densification when $\varphi > 0.1$. For $\varphi < 0.1$ (the “final” stage of densification), a slightly modified expression applies

$$-\frac{d\varphi}{dt} = 18 \left(\frac{\varphi}{6}\right)^{1/3} \frac{D_v}{r^2} \left[\frac{2\gamma}{r} \left(\frac{6}{\varphi}\right)^{1/3} - p_i \right] \frac{\Omega}{kT} + 9 \frac{\delta_b D_b}{r^3} \left[\frac{2\gamma}{r} \left(\frac{6}{\varphi}\right)^{1/3} - p_i \right] \frac{\Omega}{kT}. \quad (2)$$

Here $p_i \equiv p_o(1 - \varphi)/(19\varphi)$ and p_o is the pressure of any ambient gas that may be trapped in the pores. An algebraic “smoothing” function of porosity is usually employed to assure continuity between equations (1) and (2) at $\varphi = 0.1$. Equation (2) will not be used here, except to note that the bracketed terms become negative, and thus densification

stops, as porosity goes to zero. The precise mathematical formula for this limit is very uncertain (thus preventing quantitative estimates of the limiting p_o for any given r and φ), but the trapping effect is well known in metallurgy, where the presence of an ambient gas hinders the formation of fully dense samples [Helle *et al.*, 1985; Ashby, 1988]. In this context, the nondetection of significant quantities of nitrogen on 2005 FY₉ [Licandro *et al.*, 2006; Brown *et al.*, 2007], and thus the nonformation of “nitrogen bubbles,” appears consistent with the sintering scenario. The densification timescales computed from equation (1) as $-\varphi/(d\varphi/dt)$ for $\varphi = 0.3$ and $\varphi_0 = 0.36$ are plotted in Figure 1. We note here that the densification timescale is only weakly dependent on the choice of φ and φ_0 , compared with the much stronger dependencies on T and r and uncertainties in the material parameters; $\varphi_0 = 0.36$ corresponds to the theoretical porosity of closely packed spheres of equal size. For the temperatures likely to prevail on 2005 FY₉'s surface (20–40 K), micron-sized grains are necessary to produce densification on “seasonal” timescales comparable to 2005 FY₉'s orbital period of ~ 300 years (note that the voids, mostly forming at the physical grains' triple junctions, are likely to be somewhat smaller than the grains). We have focused on seasonal timescales, guided by the Triton/Pluto/Mars paradigm, in which the main volatile component condenses and sublimates between the atmosphere and the surface in the course of an orbital period, and thus densification, if it is to occur, must proceed on the corresponding “seasonal” (or shorter) timescales. Even when longer timescales are considered, only marginally larger grains (and the corresponding voids) are allowed, owing to the strong grain-size dependence of the densification rate in equations (1) and (2). Thus we rather conservatively estimate that the majority of voids in the putative slab will be smaller than 10 μm , and most likely micron-sized, although larger outliers are certainly possible (and in fact, desirable; see section 3). This size constraint is important for our spectral modeling, discussed next.

3. Spectral Modeling

[4] The reflectance spectra simulated in this paper have been computed as the wavelength-dependent geometric (physical) albedo defined as

$$A_p = 4 \int_{\Lambda=-\pi/2}^0 \int_{L=0}^{\pi/2} \Re(\Lambda, L, \alpha = 0) \cos \Lambda \cos^2 L dL d\Lambda \quad (3)$$

where Λ and L are the luminance longitude and latitude, respectively, and α is the solar phase angle. Throughout this paper, we set $\alpha = 0$, approximately corresponding to Earth-based observations of this distant object. For each point on the surface of the planet, the bi-directional reflectance \Re is computed as a function of incidence and emergence angles i and e , which are related to Λ and L by the formulas

$$\cos e = \cos \Lambda \cos L \quad (4)$$

$$\cos i = \cos(\Lambda + \alpha) \cos L. \quad (5)$$

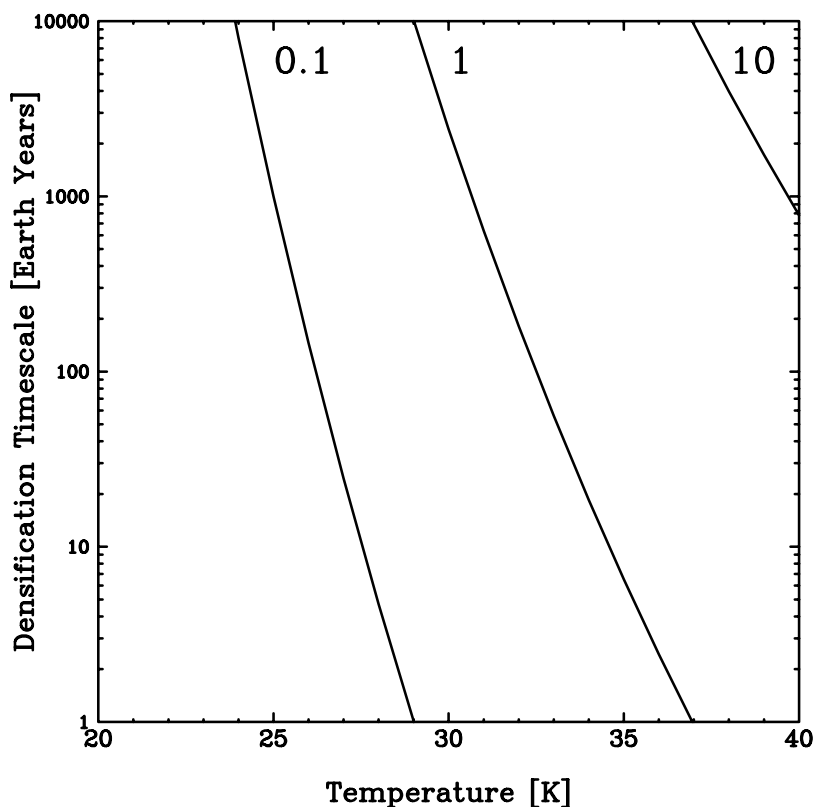


Figure 1. Densification timescale in a slab of porous methane ice containing spherical grains as a function of temperature. The curves are labeled by the grains’ radius in microns. The resulting voids are expected to be somewhat smaller.

[5] In order to gain insights into the nature of radiative transfer in a strongly forward-scattering medium, the bi-directional reflectance is computed using two approaches: the model developed by Hapke [1993, chap. 8] and explicit multiple scattering calculations carried out with the DISORT model [Stamnes *et al.*, 1988; Eluszkiewicz and Moncet, 2003]. Two basic types of surfaces have been considered:

[6] 1. Surface consisting of spherical methane ice grains in vacuo. For this case, calculations with both the Hapke and the DISORT models have been carried out.

[7] 2. Surface consisting of a methane ice slab containing spherical voids, modeled using the DISORT model in our “slab” implementation.

[8] The Hapke model is well documented elsewhere [Hapke, 1993]. Our adaptation of the DISORT model has been described in detail in two previous publications [Eluszkiewicz and Moncet, 2003; Eluszkiewicz *et al.*, 2005], but given that it is still rather new in the planetary science community, we provide an overview of its essential features in Appendix A.

[9] Figure 2 shows the spectra computed using Hapke’s and DISORT models for a methane ice layer composed of spherical grains of varying radius. For comparison, we also plot the spectrum measured by Brown *et al.* [2007], normalized to a V-band albedo p_V of 0.6. This value is at the lower end of the range $0.8^{+0.1}_{-0.2}$ estimated from the Multiband Imaging Photometer for *Spitzer* (MIPS) measurements at 24 and 70 microns [Stansberry *et al.*, 2007] although, as

discussed in section 4, estimating the albedo of 2005 FY₉ from *Spitzer* thermal data is a challenging and still unfinished task. We have adopted this rather low value as it allows for a relatively simple fit shown later (Figure 3). Adopting higher values of p_V necessitates going beyond such a simple model, in particular making the medium strongly backscattering [Brown *et al.*, 2007; Tegler *et al.*, 2007; Olkin *et al.*, 2007]. This is certainly plausible, especially if 2005 FY₉ exhibits an opposition surge. However, the existing phase curve for 2005 FY₉ is rather flat in the limited range of phase angles currently available [Rabinowitz *et al.*, 2007] and, consequently, we have opted not to consider any opposition-surge effects in this paper. As the absolute albedo and the phase curve of 2005 FY₉ become better constrained, more detailed modeling will be called for. The prospects for this are discussed in section 4.

[10] The Hapke and DISORT models are in qualitative agreement, but quantitative differences are evident in Figure 2. The DISORT model produces lower reflectivities in the regions of strong absorption, presumably through accounting for increased path lengths in the strongly forward-scattering regime. For 1-cm particles, both models give a nearly flat spectrum in the 1.7- μm region that is a distinct feature in the spectrum of 2005 FY₉ (it should be noted that, for numerical reasons, the asymmetry parameter used by DISORT has been capped at 0.95 for this particle size). This flat spectrum is the basis of the conclusion reached by Brown *et al.* [2007] concerning the likely metamorphosed state of 2005 FY₉’s surface and

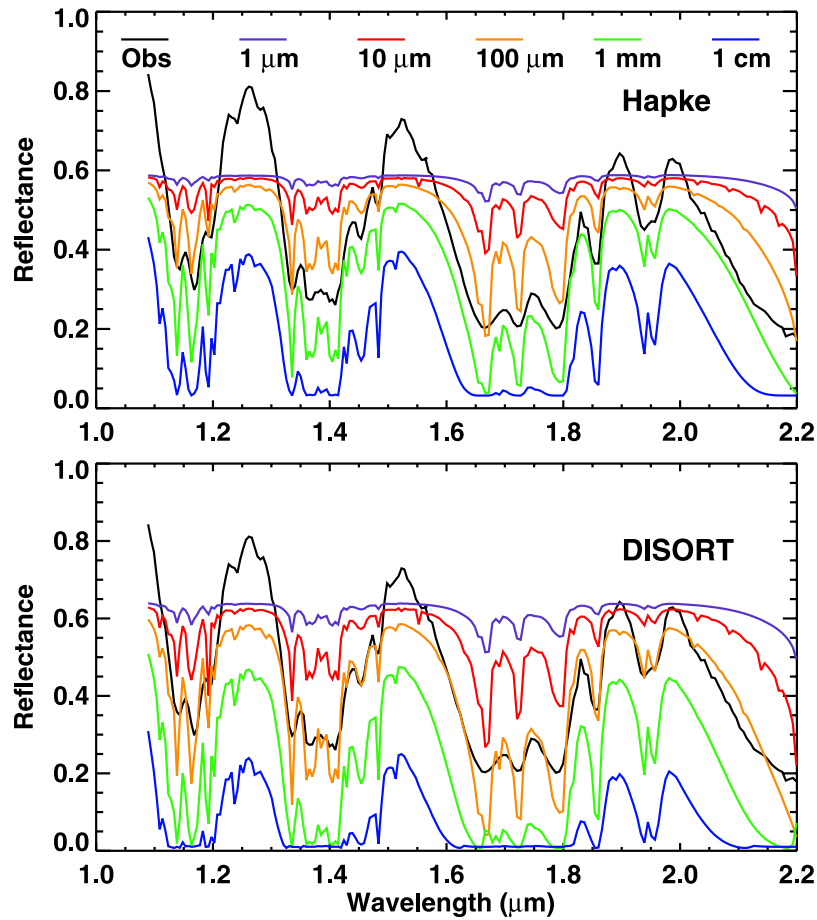


Figure 2. Black line: Measured near-IR reflectivity of 2005 FY₉, normalized to a V-band albedo p_V of 0.6. Color lines: Computed spectral reflectance $A_p(\lambda)$ of a planet covered by a 1-meter deep layer of spherical pure methane ice particles of different radius. (top) Reflectance computed using the model of *Hapke* [1993]. (bottom) Reflectance computed using the DISORT model.

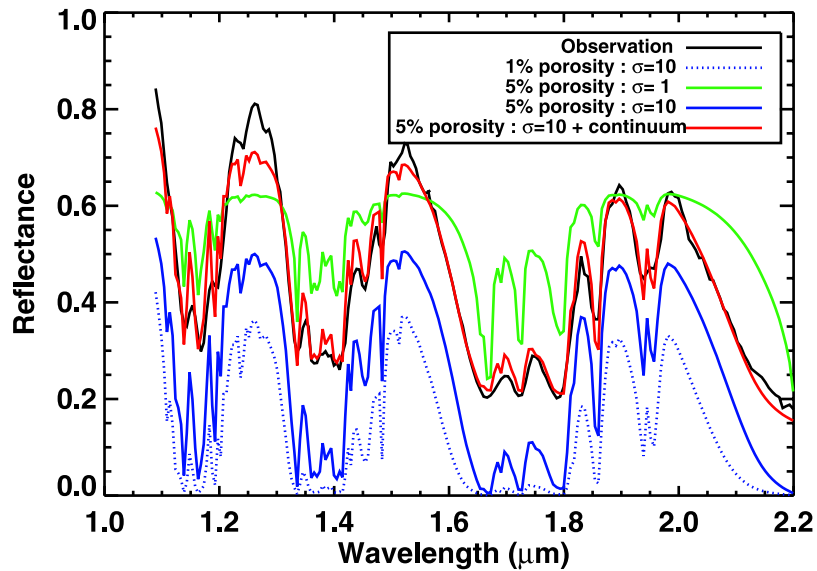


Figure 3. Black line: Measured spectrum of 2005 FY₉, normalized to $p_V=0.6$. The color lines represent spectra computed using the DISORT model for a porous slab containing spherical voids. Green: All voids with radius $0.5 \mu\text{m}$ and porosity 5%. Blue: Voids follow a lognormal distribution with mode radius $R_m = 0.5 \mu\text{m}$ and width $\sigma = 10$. The solid and dashed lines correspond to porosities of 5 and 1%, respectively. Red: Same as blue with 5% porosity, but with the added sloping continuum.

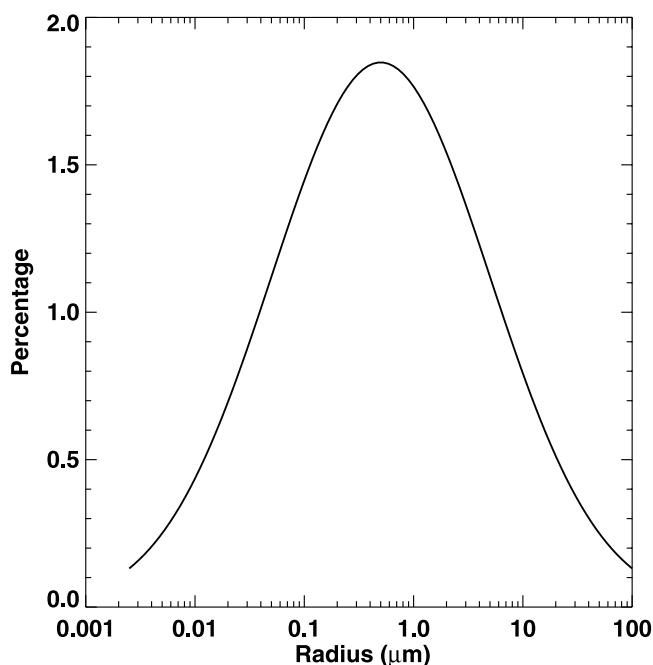


Figure 4. Distribution of void radii used in the DISORT calculations.

it has been used as an end-member case in a 2-component granular model constructed by *Brown et al.* [2007] that provides a very good fit to the measured spectrum (the other component being a sloping continuum). The flatness of the spectrum in the region of strong absorption is a consequence of reaching the geometric optics limit.

[11] However, it is clear, as has been recognized by *Brown et al.* [2007] and *Tegler et al.* [2007], that golf-ball sized particles of methane ice do not exist on 2005 FY₉'s surface and they are merely indicative of long path lengths prevailing in a densified slab of solid methane. Consequently, the main objective of this paper is to determine whether an end-member spectrum similar to the blue lines in Figure 2 can indeed be obtained using a porous slab model with realistic assumptions about the size of the voids. For this purpose, we have experimented with a wide range of porosities and void sizes smaller than 10 μm. The upper limit on the dominant void size is consistent with the sizes required to produce a densified slab on “seasonal” time-scales comparable to 2005 FY₉'s orbital period. Representative spectra are shown in Figure 3, which illustrates the following cases:

[12] 1. Green line: 5% porosity, with all voids having the same radius of 0.5 μm.

[13] 2. Blue lines: Voids follow a lognormal distribution of the form

$$N_i = \frac{N}{r_i \sqrt{2\pi \ln \sigma}} \exp \left[-\frac{\ln^2 (r_i/R_m)}{2 \ln^2 \sigma} \right] \quad (6)$$

where

- N_i number of voids with radius r_i per unit volume;
- N total number of voids per unit volume;
- R_m mode radius;

σ distribution width ($\sigma = 1$ corresponds to a mono-disperse distribution).

The distribution adopted in Figure 3 corresponds to $R_m = 0.5 \mu\text{m}$ and $\sigma = 10$ and is shown in Figure 4. The blue solid and blue dashed lines in Figure 3 correspond to porosities of 5 and 1%, respectively.

[14] 3. Red line: Best fit. It combines in the 90–10% ratio the spectrum computed for 5% porosity and 0.5-μm voids lognormally distributed (i.e., solid blue line) and a sloping continuum with a reflectance of 0.93 at 1 μm and 0.48 at 2.2 μm. The slope of the continuum has been determined through least squares fitting.

[15] The main conclusions reached from Figure 3 (and numerous additional runs) are as follows:

[16] 1. The slab model can reproduce a flat spectrum in the 1.6–1.8 μm region for small porosities (<5%) and micron-sized voids that follow a broad size distribution. The spectrum for porosity of 1% closely resembles the 1-cm spectra in Figure 2.

[17] 2. Including a distribution of void sizes is necessary for producing flat spectra.

[18] 3. A simple 2-component model containing the porous slab and a sloping continuum is capable of producing a semiquantitative fit to the observed spectra (except beyond 2.2 μm, where additional absorbers have been detected). This is consistent with the findings of *Brown et al.* [2007]. The remaining discrepancies between the black and red curves in Figure 3 could be related to (and possibly ameliorated by) subtle effects stemming from the interplay between the assumed porosity, void size distribution, and temperature dependence of the refractive indices for methane ice [*Grundy et al.*, 2002].

[19] 4. We have not been able to fit the spectra scaled to a high visible albedo ($p_V > 0.7$), without arbitrarily changing the optical properties of the slab, particularly making the voids strongly backscattering. The discrepancies were largest away from the absorption peaks and this indicates, if p_V is indeed at the high end of the current estimates, that an opposition surge does in fact occur on 2005 FY₉. *Olkin et al.* [2007] illustrate the sensitivity of their synthetic Pluto spectra to the assumed asymmetry parameter and find, in agreement with our results, that the inclusion of backscattering is necessary for the simulation of continuum levels.

4. Discussion

[20] Clearly, a definitive quantitative modeling of 2005 FY₉'s spectra is not yet possible. However, even at this stage, the slab model offers a physically based approach applicable to the visible, near-IR, and thermal infrared spectral regions, and has the potential to provide quantitative insights into the state of the 2005 FY₉'s surface. Although the focus of this paper has been on modeling the near-IR spectra, the slab model can easily be applied in the visible and thermal spectral ranges, without resorting to unrealistic assumptions about the size of scatterers. In fact, the visible spectrum calculated for our best case (i.e., 5% porosity, 0.5-μm voids lognormally distributed) exhibits all the strong absorption features evident in the published spectra [*Brown et al.*, 2007; *Tegler et al.*, 2007]. A quantitative modeling of these spectra is beyond the scope of this

paper, as this would require an explicit modeling of the “continuum” component used in Figure 3. This component would have to be “red” in order to match the slope present in the visible spectra and an explicit model will have to make specific assumptions about the composition and granularity of this component (e.g., tholins versus silicates), in addition to accounting for the absorption features caused by solid ethane at wavelengths longer than $2.2 \mu\text{m}$ [Brown *et al.*, 2007]. Explicit models will become possible (in fact, necessary) when measurements of 2005 FY₉ at longer wavelengths (up to $8 \mu\text{m}$) with the Infrared Array Camera (IRAC) on *Spitzer* [Emery *et al.*, 2007] become available.

[21] As a natural by-product of applying the slab model to match the visible/near-IR spectra, physically consistent values of the visible phase integral q and the thermal emissivity ε could in principle be obtained. This, in turn, should lead to better size and albedo estimates from the *Spitzer*/MIPS thermal measurements, since the precise values of q and ε have a large impact on the estimates of the visible albedo p_V for high-albedo objects such as 2005 FY₉ [Stansberry *et al.*, 2007]. On the other hand, as noted in section 3, the physical parameters entering the slab model that give a good fit to the observed visible/near-IR spectra depend on the assumed value of p_V : this suggests an iterative approach for a self-consistent determination of p_V (and size) for 2005 FY₉ and other volatile-rich Trans-Neptunian Objects. Ideally, the product qp_V , as computed by the slab model, should be equal to the bolometric albedo estimated from *Spitzer* (using the slab-model based value of ε). In this approach, the slab model would provide the link between the composition and microphysical state of the surface and its solar reflectance and thermal emissivity. The resulting compositional, albedo, and size estimates would be more robust than those derived from ad hoc assumptions about emission and scattering behavior and would lay a solid physical foundation for future studies of these fascinating bodies.

[22] Other elements of a consistent “story” are also emerging. The absence of an opposition surge [Rabinowitz *et al.*, 2007] appears consistent with the widespread presence of a densified methane ice, as the surge is commonly attributed to shadow-hiding and/or coherent backscatter in a fluffy medium. The absence of a surge could, in fact, be taken as a falsifiable prediction from the slab interpretation. An Earth-based test of this prediction is a long way off (the solar phase angle for Earth-based observations of 2005 FY₉ will not diminish to 0.15 deg until 2087 AD and true opposition will only occur early next century), but earlier spacecraft observations are conceivable. Furthermore, the presence of a slab could lower 2005 FY₉’s albedo relative to, say, Pluto (and thus make it more in line with the value of 0.6 adopted in this paper), as it would allow an underlying darker substrate to be partially seen. This effect has been postulated to explain the dark appearance of Triton’s northern hemisphere at the time of the Voyager flyby [Moore and Spencer, 1990; see also Helfenstein *et al.*, 1992 and Lee *et al.*, 1992] and of regions in the polar caps on Mars [Kieffer *et al.*, 2000], with the presence of densified layers of nitrogen and CO₂ ice being responsible in the two cases, respectively [Eluszkiewicz, 1991, 1993]. It should be noted that in the absence of backscattering effects, 0.7 is the theoretical upper limit to the albedo of a spherical planet

[Hapke, 1993, chap. 10.E.5]. Triton’s albedo is somewhat higher than this, but it is variable [Hicks and Buratti, 2004]. Early observations produced no evidence of an opposition surge on Triton for phase angles as low as 0.05 deg [Gougen *et al.*, 1989], consistent with a slab-like texture [Eluszkiewicz, 1991], while more recent data indicate a surge for phase angles less than 0.15 deg [Cobb *et al.*, 2001; B. Buratti, personal communication, 2007]. On Triton, the variability evident in the telescopic observations (both with regard to the albedo and the absence/presence of an opposition surge) could be attributed to the deposition of fresh nitrogen frost, something less likely to occur in the less volatile methane ice on 2005 FY₉. A methane ice slab would affect the energy balance of the surface, e.g., through the formation of a solid-state greenhouse effect [e.g., Kirk *et al.*, 1990], and thus its interactions with any atmosphere that may be present. Conversely, the nondetection of nitrogen on 2005 FY₉, possibly related to the object’s intermediate size between volatile retention and loss [Schaller and Brown, 2007], is consistent with the formation of an impermeable methane ice slab. The presence of nitrogen gas in significant quantities would slow the densification process through a volumetric dilution effect, the stirring of methane grains by nitrogen winds, and “bubble trapping” in the final stage (section 2). The presence of an ambient gas, air, is in fact the main reason pressureless sintering does not lead to densification in the terrestrial snow. In this context, the slab interpretation offers another falsifiable prediction applicable to volatile-rich KBOs in general, namely that it is unlikely to find very long (centimeters or more) spectroscopic path lengths in both nitrogen and methane ice simultaneously on the same object. Finally, and perhaps incidentally, we note that a lognormal grain-size distribution is a popular concept in metallurgy in situations of “normal” growth [Hillert, 1965], although it is not clear whether the evolution of void sizes on 2005 FY₉ (possibly occurring in a thermal gradient) follows a similar pattern. These intriguing aspects remain to be investigated in the future, as new observational data become available.

Appendix A: Slab Model

A1. Mie Solution

[23] The slab model represents the medium as a matrix (in this case, solid CH₄) that contains spherical voids acting as scatterers (although it should be noted that the model can easily be run in the “granular” mode by assuming a vacuum matrix and spherical particles). In order to solve the radiative transfer equation in this medium, the model relies on the Mie solution for a spherical particle embedded in an absorbing host matrix. As noted by several authors [Yang *et al.*, 2002, and references therein], this solution and the resulting single-scattering properties, i.e., the asymmetry factor g (defined as the first moment of the phase function, i.e., $g = (1/2) \int_0^\pi p(\cos\theta)\sin\theta d\theta$) and the single scattering albedo ϖ_o , cannot be obtained by employing the complex refractive indices for the particle and the matrix as input to a conventional Mie code (mainly as a result of different boundary conditions for the Maxwell equations). Consequently, Yang *et al.* [2002] have considered the general problem when the refractive indices for the particle and the medium have arbitrary values and the slab model employs

their code to compute g and ϖ_o (including standard expressions to account for polydisperse size distributions [e.g., Yang *et al.*, 2002]). For pure voids considered in this paper, the values of ϖ_o are identically 1 (in the granular mode, $\varpi_o < 1$ generally). In addition to computing g , the Mie code outputs the values of the scattering and absorption efficiency factors Q_s and Q_a and these are used to compute the effective single-scattering properties that enter the radiative transfer equation. The exact procedure for doing this is described in the next subsection.

A2. Radiative Transfer

[24] Once the single-scattering properties of the voids have been calculated, the slab model employs the publicly available DISORT code [Stamnes *et al.*, 1988] to solve the equation of radiative transfer. Under the assumptions of plane-parallel geometry and azimuthal symmetry, this equation reads

$$\mu \frac{dI_\nu(\tau_\nu, \mu)}{d\tau} = I_\nu(\tau_\nu, \mu) - S_\nu(\tau_\nu, \mu) \quad (\text{A1})$$

where $I_\nu(\tau_\nu, \mu)$ is the specific intensity (radiance) at frequency ν at optical depth τ_ν (measured perpendicular to the surface) and along direction $\mu \equiv \cos e$ (where e is the emergence angle). Henceforth, the subscript “ ν ” will be omitted for simplicity. S is the source function given by

$$S(\tau, \mu) = \frac{\varpi_o^{\text{eff}}}{2} \int_{-1}^1 p(\tau, \mu; \mu') I(\tau, \mu') d\mu' + Q(\tau, \mu) \quad (\text{A2})$$

where is $\varpi_o^{\text{eff}}(\tau)$ the frequency-dependent effective single-scattering albedo (see below) and $p(\tau, \mu, \mu')$ is the phase function. In the solar spectral region relevant to this paper

$$Q(\tau, \mu) = \frac{\varpi_o^{\text{eff}}(\tau) I_o}{4\pi} p(\tau, \mu; -\mu_o) e^{-\tau/\mu_o} \quad (\text{A3})$$

where $\mu_o I_o$ is the solar flux incident in direction $\mu_o \equiv \cos i$ (i is the incidence angle). The bi-directional reflectance entering equation (3) is defined as $\mathfrak{R}(\mu_o, \mu) \equiv I(0, \mu) I_o$. At the interface between the slab and any underlying “ground,” a Lambertian surface with an albedo of 0.2 is assumed (although our results are insensitive to this value). In this initial application of the model to 2005 FY₉, the simplest case of a homogeneous layer has been considered, i.e., the single-scattering properties are assumed to be independent of optical depth, but the model can handle the more general vertically inhomogeneous case without difficulty. We also note that we have incorporated into the slab model the formalism of Hapke [1993, chap. 12] to account for macroscopic roughness, although this produced only minor changes in our synthetic spectra and is not illustrated in this paper.

[25] In this work, the phase function has been approximated by the Henyey-Greenstein formula [Hapke, 1993, equation (6.7)] characterized by the effective asymmetry factor g^{eff} derived from the Mie calculations. Specifically, to account for the two-component nature of the medium (matrix + voids in the “slab” case or vacuum + grains in

the traditional “granular” approach), the effective single scattering albedo and asymmetry factor are computed as

$$\varpi_o^{\text{eff}} = \frac{\tau_s^p}{\tau_s^p + \tau_a^p + \tau_a^m} \quad (\text{A4})$$

$$g^{\text{eff}} = g^p \quad (\text{A5})$$

where “ p ” and “ m ” stand for “particle” and “matrix,” respectively (i.e., void and ice matrix in the slab case and grain and vacuum in the granular case). These expressions are a special case of the mixing formulas presented by Hapke [1993, chap. 10.F] and Eluszkiewicz and Moncet [2003]. The scattering and absorption optical depths are computed using the expressions

$$\tau_a^m = (1 - \varphi) L \frac{4\pi m_i}{\lambda} \quad (\text{A6})$$

$$\tau_{s,a}^p = \frac{\varphi L}{\frac{4}{3}\pi r^3} Q_{s,a}^p \pi r^2 \quad (\text{A7})$$

where L is the total thickness of the slab (assumed to be 1 meter, although the results are insensitive to its precise value), φ is the porosity (or particle abundance by volume in the granular case), m_i is the imaginary index of refraction for solid methane, λ is the wavelength, and $Q_{s,a}^p$ is the scattering/absorption efficiency factor of the particle derived from the Mie calculations. Note that for voids $\tau_a^p \equiv 0$, while in the granular case $\tau_a^m \equiv 0$. In this work, the refractive indices for pure methane ice at 30 K [Grundy *et al.*, 2002] have been adopted.

[26] **Acknowledgment.** Work at AER has been supported by the NASA Planetary Geology and Geophysics Program.

References

- Ashby, M. F. (1988), *Background Reading: Hot Isostatic Pressing and Sintering*, Eng. Dep., Univ. of Cambridge, Cambridge, UK.
- Barucci, M. A., D. P. Cruikshank, E. Dotto, F. Merlin, F. Poulet, C. Dalle Ore, S. Fornasier, and C. de Bergh (2005), Is Sedna another Triton?, *Astron. Astrophys.*, 439, L1–L4.
- Brown, M. E., K. M. Barkume, G. A. Blake, E. L. Schaler, D. L. Rabinowitz, H. G. Roe, and C. A. Trujillo (2007), Methane and ethane on the bright Kuiper Belt Object 2005 FY₉, *Astron. J.*, 133, 284–289.
- Cobb, B. E., B. J. Buratti, M. D. Hicks, M. Garske, and J. Ward (2001), The BVRI lightcurve and opposition phase curve of Triton in 2000, *Bull. Am. Astron. Soc.*, 33, 1130.
- Cruikshank, D. P., R. H. Brown, and R. N. Clark (1984), Nitrogen on Triton, *Icarus*, 58, 293–305.
- Eluszkiewicz, J. (1991), On the microphysical state of the surface of Triton, *J. Geophys. Res.*, 96, 19,217–19,229.
- Eluszkiewicz, J. (1993), On the microphysical state of the martian seasonal caps, *Icarus*, 103, 43–48.
- Eluszkiewicz, J., and J.-L. Moncet (2003), A coupled microphysical/radiative transfer model of albedo and emissivity of planetary surfaces covered by volatile ices, *Icarus*, 166, 375–384.
- Eluszkiewicz, J., J. Leliwa-Kopystynski, and K. J. Kossacki (1998), Metamorphism of solar system ices, in *Solar System Ices*, edited by B. Schmitt *et al.*, pp. 119–138, Kluwer Acad., New York.
- Eluszkiewicz, J., J.-L. Moncet, T. N. Titus, and G. B. Hansen (2005), A microphysically-based approach to modeling emissivity and albedo of the martian seasonal caps, *Icarus*, 174, 524–534.
- Emery, J. P., C. M. Dalle Ore, D. P. Cruikshank, Y. R. Fernandez, D. E. Trilling, and J. A. Stansberry (2007), Ices on (90377) Sedna: Confirmation and compositional constraints, *Astron. Astrophys.*, 466, 395–398.

- Gougen, J. D., H. B. Hammel, and R. H. Brown (1989), V photometry of Titania, Oberon, and Triton, *Icarus*, *77*, 239–247.
- Grundy, W. M., B. Schmitt, and E. Quirico (2002), The temperature-dependent spectrum of methane ice I between 0.7 and 5 μm and opportunities for near-infrared remote thermometry, *Icarus*, *155*, 486–496.
- Hapke, B. (1993), *Theory of Reflectance Spectroscopy*, Cambridge Univ. Press, Cambridge, UK.
- Helfenstein, P., J. Veverka, D. McCarthy, P. Lee, and P. Hillier (1992), Large quasi-circular features beneath frost on Triton, *Science*, *255*, 824–826.
- Helle, A. S., K. E. Easterling, and M. F. Ashby (1985), Hot-isostatic pressing diagrams: New developments, *Acta Metall.*, *33*, 2163–2174.
- Hicks, M. D., and B. J. Buratti (2004), The spectral variability of Triton from 1997–2000, *Icarus*, *171*, 210–218.
- Hillert, M. (1965), On the theory of normal and abnormal grain growth, *Acta Metall.*, *13*, 227–238.
- Kieffer, H. H., T. N. Titus, K. F. Mullins, and P. R. Christensen (2000), Mars south polar spring and summer behavior observed by TES: Seasonal cap evolution controlled by frost grain size, *J. Geophys. Res.*, *105*, 9653–9699.
- Kirk, R. L., R. H. Brown, and L. A. Soderblom (1990), Subsurface energy storage and transport for solar-powered geysers on Triton, *Science*, *250*, 424–429.
- Lee, P., P. Helfenstein, J. Veverka, and D. McCarthy (1992), Anomalous-scattering region on Triton, *Icarus*, *99*, 82–97.
- Licandro, J., N. Pinilla-Alonso, M. Pedani, E. Oliva, G. P. Tozzi, and W. M. Grundy (2006), The methane ice rich surface of large TNO 2005 FY₉: A Pluto-twin in the trans-Neptunian belt?, *Astron. Astrophys.*, *445*, L35–L38.
- Moore, J. M., and J. R. Spencer (1990), Koyaanismuuyaw: The hypothesis of a perennially dichotomous Triton, *Geophys. Res. Lett.*, *17*, 1757–1760.
- Olkin, C. B., E. F. Young, L. A. Young, W. Grundy, B. Schmitt, A. Tokunaga, T. Owen, T. Rousch, and H. Terada (2007), Pluto's spectrum from 1.0 to 4.2 μm : Implications for surface properties, *Astron. J.*, *133*, 420–431.
- Owen, T. C., T. L. Rousch, D. P. Cruikshank, J. L. Elliot, L. A. Young, C. de Bergh, B. Schmitt, T. R. Geballe, R. H. Brown, and M. J. Bartholomew (1993), Surface ices and the atmospheric composition of Pluto, *Science*, *261*, 745–748.
- Rabinowitz, D. L., B. E. Schaefer, and S. Tourtellotte (2007), The diverse solar phase curves of distant icy bodies. I. Photometric observations of 18 Trans-Neptunian Objects, 7 Centaurs, and Nereid, *Astron. J.*, *133*, 26–43.
- Schaller, E. L., and M. E. Brown (2007), Volatile loss and retention on Kuiper Belt Objects, *Astrophys. J. Lett.*, *659*, L61–L64.
- Stammes, K., S.-C. Tsay, W. Wiscombe, and K. Jayaweera (1988), Numerically stable algorithm for discrete-ordinate method radiative transfer in multiple-scattering and emitting layered media, *Appl. Opt.*, *27*, 2502–2509.
- Stansberry, J., W. Grundy, M. Brown, D. Cruikshank, J. Spencer, D. Trilling, and J.-L. Margot (2007), Physical properties of Kuiper Belt Objects and Centaurs: *Spitzer Space Telescope* constraints, in *The Solar System Beyond Neptune*, edited by A. Barucci et al., Univ. of Ariz. Press, Tucson, in press.
- Swinkels, F. B., and M. F. Ashby (1981), A second report on sintering diagrams, *Acta Metall.*, *29*, 259–281.
- Tegler, S. C., W. M. Grundy, W. Romanishin, G. J. Consolmagno, K. Mogren, and F. Vilas (2007), Optical spectroscopy of the large Kuiper Belt Objects 136472 (2005 FY₉) and 136108 (2003 EL61), *Astron. J.*, *131*, 526–530.
- Yang, P., et al. (2002), Inherent and apparent scattering properties of coated or uncoated spheres embedded in an absorbing host medium, *Appl. Opt.*, *41*, 2740–2759.

M. E. Brown, Division of Geological and Planetary Sciences, California Institute of Technology, Pasadena, CA 91125, USA.

K. Cady-Pereira and J. Eluszkiewicz, Atmospheric and Environmental Research, Inc., 131 Hartwell Avenue, Lexington, MA 02421, USA. (jel@acr.com)

J. A. Stansberry, Steward Observatory, University of Arizona, Tucson, AZ 85721, USA.